

# Automated Lung Disease Detection and Classification Using Quantum Glowworm Swarm Optimizer with Quasi Recurrent Neural Network on Chest X-Ray Images

<sup>1,\*</sup>Ms. Vidyasri S., <sup>2</sup>Dr. Saravanan S.

<sup>1</sup>Research Scholar, Department of Computer and Information Science,  
Faculty of Science, Annamalai University, Annamalai Nagar, Chidambaram,  
Tamil Nadu, India.

thirukamusaipriya1991@gmail.com

<sup>2</sup>Assistant Professor/Programmer, Department of Computer and Information Science,  
Faculty of Science, Annamalai University, Annamalai Nagar, Chidambaram,  
Tamil Nadu, India.

aucissaran@gmail.com

**Abstract**— Lung diseases or otherwise called respiratory diseases are airborne diseases that affect the lungs and the other tissues of the lungs. Tuberculosis, Coronavirus Disease 2019 (COVID-19), and Pneumonia are a few instances of lung diseases. If the lung disease is diagnosed and treated in the initial stage, the chances of recovery rate and long-term survival rates can be increased. Usually, lung disease is identified by Chest X-Ray (CXR) image examination, skin test, sputum sample test, Computed Tomography (CT) scan examination, and blood test. Because of its non-invasive and convenient evaluation for overall outcomes of the chest situation, Lung disease can be detected by specialized radiologists on CXR images. In recent times, Deep Learning (DL) applies to medical images for disease detection and has proved an effective technique for detecting disease. The recent advancement of DL supports the detection and classification of lung diseases in medicinal imaging. This article presents an Automated Lung Disease Detection Using Quantum Glowworm Swarm Optimization with Quasi Recurrent Neural Network (QGSO-QRNN) model on CXR imaging. The presented QGSO-QRNN technique focuses on the identification of lung diseases using DL concepts. To accomplish this, the presented QGSO-QRNN technique initially performs image pre-processing by the use of the Gaussian Filtering (GF) technique. Besides, the Faster SqueezeNet approach is exploited for feature vector generation. Finally, the QRNN model is applied for precise classification of lung diseases with the QGSO technique as a hyperparameter optimizer. The investigational assessment of the QGSO-QRNN technique is examined by employing standard medical datasets and the outputs display the promising performance of the QGSO-QRNN technique over other existing techniques by means of diverse measures.

**Keywords**- Lung diseases; Computer-aided diagnosis; Deep learning; Quantum glowworm swarm optimizer; Quasi recurrent neural network

## I. INTRODUCTION

Pulmonary ailment is one among the familiar diseases around the globe and this comprises COVID-19, tuberculosis, chronic obstructive lung ailment, asthma, pneumonia, fibrosis, etc. Sensible analysis of these lung diseases is very crucial [1]. The consequences of these diseases on well-being are hastily growing due to the modifications to the atmosphere, lifestyle, climatic variations, and further aspects. The dangers associated with these lung diseases are tremendous, particularly in emerging and low-middle-income nations, where persons in million are fronting scarcity and air contamination [2]. According to the assessment of WHO, more than 4 million premature loss of life happens per annum ranging from domestic air pollution-associated diseases that include pneumonia, and asthma. Henceforth, it becomes essential to take the required

steps to reduce carbon emanation and air pollution [3]. It is also crucial to adopt effective diagnostic methods that can support in discovering lung diseases. Earlier valuation and analysis can substantially diminish lung diseases' life-threatening nature and advance the suffering patients' value of life [4]. In recent medical image techniques, imaging assessments are tremendously influential utensils that can help physicians in diagnosing a variety of conditions. The utmost generally used image techniques are CT, and CXR imaging. These are analytical tools in allowing physicians to look at the internal structure of the human body by not involving surgery [5]. Discovering pulmonary ailment is presently accomplished by a professional radiologist through CXR image inspection because of its non-invasive valuation and comfort for total discoveries of the chest conditions in short. This is also appropriate for inspection follow-ups as disease variations can be detected more

initially and effortlessly [6]. Still, there was a prevalent human mistake that might be produced by the misconception of CXR images because of the convolutional anatomical structures of the chest. Hence, Computer Aided Diagnosis structure (CAD) is used in assisting radiologists to solve clinical verdicts with accurate analysis and in minimizing mistakes [7].

Lately, CAD frameworks support a swift, automatic analysis employing Graphical Processing Unit (GPU) by processing medical images. In our best intelligence, DL, and Machine Learning (ML) style has been employed in several CAD frameworks and the applications of several medical imaging like lung diseases [8]. Recently, Convolutional Neural Networks (CNNs) have generated the most capable outcomes in categorizing radiological images. CNNs are DL algorithms that are employed in several applications, including the cataloguing of images. These merits have inspired our attempt in recommending a DL model for the diagnosis of lung diseases. The hyperparameters of CNN have a crucial impact on the performance of the network due to their direct control over the training method [9]. Selecting a suitable hyperparameter act as a crucial part of the CNN training. For example, in case of a low learning rate, there is a possibility of the network losing critical information in the data. On the contrary, in case of a high learning rate, this may lead the model to converge very fast [10]. Hence, for appropriate training and maximum performance outcomes, there comes a requirement of optimizing the hyperparameters of CNNs.

This article presents an Automated Lung Disease Detection Using Quantum Glowworm Swarm Optimization with Quasi Recurrent Neural Network (QGSO-QRNN) model on CXR imaging. The presented QGSO-QRNN technique focuses on the identification of lung diseases using DL concepts. To accomplish this, the presented QGSO-QRNN technique initially performs image pre-processing by the use of the Gaussian Filtering (GF) technique. Besides, the Faster SqueezeNet approach is exploited for feature vector generation. Finally, the QRNN model is applied for precise classification of lung diseases with the QGSO technique as a hyperparameter optimizer. The investigational assessment of the QGSO-QRNN technique is examined by employing standard medical datasets.

## II. RELATED WORKS

In [11], the authors devised a new lung disease prediction structure utilizing a hybrid bidirectional LSTM (BiDLSTM)-Mask Region-Based CNN (Mask-RCNN) technique. For optimizing the convergence issues and scalability in the Mask-RCNN method, the Crystal technique was utilized. Utilizing the BiDLSTM method, long-ranging dependency for pulmonary ailment anticipation was done, this BiDLSTM was linked to the FC layer of the Mask RCNN approach. Kim et al. [12] introduced a DL technique using a TL method for executing the classification process of lung disease on CXR imageries for

enhancing the accuracy and efficiency of CADs' diagnostic performances. This technique refers to a 1-step, comprehensive learning that indicates that raw CXR imaging are given as an input straightly into a DL method (Efficient Net v2-M) to derive their significant attributes in finding ailment classes.

Ravi et al. [13] devise a multichannel DL methodology for detecting lung disease by employing CXRs. The EfficientNetB2, EfficientNetB0, and EfficientNetB1 pretrained models are few multichannel methods utilized. The Efficient Net methods were merged. Then, the merged features were sent into multiple non-linear FC layers. Eventually, for lung disease detection, features are sent into a stacked ensemble learning classifier. The SVM and RF are inherent in a stacked ensemble learning classifier in the initial phase and LR in the next phase for detecting pulmonary diseases. Kabiraj et al. [14] devised a CXR-Ultraneet to identify and classify 13 thoracic lung diseases from CX-ray by multi-class cross-entropy loss function over compound scaling structure by employing EfficientNet as baseline.

In [15], the authors presented a DL structure for multi-class classification of Tuberculosis, Pneumonia, and most recently COVID-19 Lung Cancer, and Lung Opacity. For classification, the authors used a pre-trained model, VGG19 following 3 blocks of CNN as an FC and feature extraction network at the classification phase. In [16], the authors built a multi-scale adaptive RNN (MARnet) for finding CXR imagery of pulmonary ailments. For making better model for image feature extraction, the authors cross-transfer the data derived by residual block and data derived by the adaptive framework to diverse layers, evading the lessening effects of residual structures on adaptive function.

## III. THE PROPOSED MODEL

In this research, we have presented a new QGSO-QRNN model for recognizing and classifying lung ailments on the CXR imaging. It encompasses a sequence of procedures namely GF-based pre-processing, Faster SqueezeNet-based feature extractor, QGSO-based tuning process, and QRNN-based classifying. Fig. 1 shows the comprehensive procedure of the QGSO-QRNN method.

A. Image Pre-processing

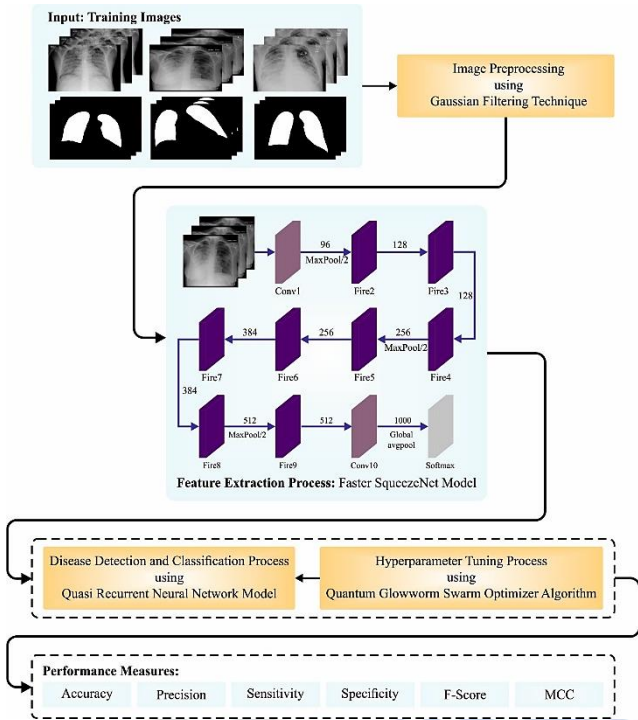


Figure 1. Overall procedure of the QGSO-QRNN approach

Mainly, the proposed QGSO-QRNN method initially pre-processed the input imaging via the GF method. It is a linear smooth filter, in which the weight was chosen for smoothing effort dependent upon Gaussian function summary [17]. GF in the non-stop space and is resolved with outcome equation as,

$$h(m, n) = \left( \frac{1}{\sqrt{2\pi\sigma}} e^{-\frac{m^2}{2\sigma^2}} \right) \times \left( \frac{1}{\sqrt{2\pi\sigma}} e^{-\frac{n^2}{2\sigma^2}} \right) \quad (1)$$

In 1-D GF is impulse response,

$$g(x) = \sqrt{\frac{a}{\pi}} e^{-ax^2} \quad (2)$$

This equation is also formulated by the Standard Deviation (SD) as a parameter.

$$g(x) = \frac{1}{\sqrt{2\pi}\sigma} e^{-\frac{x^2}{2\sigma^2}} \quad (3)$$

Although, the SDs are stated in their physical units, i.e., time and frequency by means of seconds and Hertz.

B. Feature Extraction

In this research, the Faster SqueezeNet approach is utilized for effectually generating the feature vector. The Faster SqueezeNet was suggested to enhance the classifier achievement of the electronic module [18]. Further, BatchNorm and the remaining frameworks are used for preventing overfitting. As DenseNet, it Simultaneously utilizes concat for interconnecting different layers to enhance the primary layer’s expressiveness from the networking. The Fast SqueezeNet has global average pooling, a single BatchNorm layer, three-block layers, and 4

complex layering. The Fast SqueezeNet is enhanced mainly in the succeeding way: For improving the flow of data amid layers, it imitates DenseNet architecture and presents dissimilar mode of connection. It has a pooling layer and a fire unit, and ultimately, the 2 concat layering’s were related with the subsequent complex layers. The current layer attains every feature mapping of the prior layer, and it is employed  $[x_0, \dots, x_{l-1}]$  as input value; and then,  $x_l$  is illustrated as:

$$x_l = H_l ([x_0, x_1, \dots, x_{l-1}]) \quad (4)$$

where  $[x_0, x_1, \dots, x_{l-1}]$  indicates the relation of the feature graph generated from the layer range  $\{0, 1, \dots, l-1\}$  and  $H_l$  incorporate various input values. By not improving network parameters, the efficacy of the networking has enhanced from the initial phases, and concurrently, some 2-layer networks are directly connected to data. It can be studied in the ResNet and presented in different structure block that has fire modules and pooling layers for ensuring optimal network convergence. Finally, once the 2 layers are added, they are connected with the next convolutional layer.

In ResNet, the shortcut link utilizes identity map representing the convolutional stack’s input was fed to the convolution stack’s output. The desired fundamental map illustrated as  $H(x)$ , contemplate that stacked non-linear layer proper another map of  $F(x) := H(x) - x$ . A novel map was a reform as to  $F(x) + x$  that is realized by a structure namely a shortcut connection from the real encoding system. Mostly, the shortcut connection will skip numerous layers. Hence, it utilizes the remaining ResNet construction to resolve the issue of gradient disappearance without enhancing the number of networking variables.

C. Hyperparameter Tuning

To optimize the hyperparameters of the Quasi recurrent neural network model, the QGSO algorithm is used. QGSO is a new swarm optimizing technique inspired by the luminescent features of fireflies [19]. Now, the glowworm swarm is dispersed in solution space, and fluorescence intensity is applied to the FF of the glowworm’s position. The location of a glowworm is based on the brightness intensity which signifies the FF value is maximum. Likewise, glowworm has a dynamic line of vision that can be represented as a decision domain, in which the range was pertinent to the density of neighbouring nodes. When the maximal amount of iterating is attained, the glowworm is located at better a location. Increment the neighbour set, upgrading the fluorescein concentration, updating movement probabilities, the glowworm position upgradation, and enhancing the decision domain radius are the 5 phases of GSO. The mathematical expression of the fluorescein concentration increment method can be given as follows:

$$l_i(t) = (1 - \alpha)l_i(t - 1) + \beta f(x_i(t)) \quad (5)$$

In Eq. (5),  $\alpha$  signifies fluorescein volatilization coefficient,  $l_i(t)$  indicates fluorescein concentration of  $i$ -th glowworms at

time,  $\beta$  represents the fluorescein enhancing factor,  $x_i(t)$  describes the position of  $i$ -th glowworms at  $t$  time and  $f(x)$  refers the FF value. Thus, an increment in the neighbour set can be represented as

$$N_i(t) = \{j: \|\chi_j(t) - x_i(t)\| < r_d^i; l_i(f) < l_j(t)\} \quad (6)$$

In Eq. (6),  $r_d^i(t)$  denotes the decision domain radius of  $i$ -th glowworms at  $t$  moment.  $N_i(t)$  indicates a neighbour set of  $i$ -th glowworms at  $t$  time. Hence, improving the decision domain radius method can be defined by

$$r_d^i(t+1) = \min \left\{ r_s, \max \{r_d^i(t) + \gamma(n_i - |N_i(t)|)\} \right\} \quad (7)$$

In Eq. (7),  $n_i$  signifies the adjacent threshold,  $\gamma$  implies the decision domain's rate of change, and  $r_s$  denotes the perceived radius of the glowworm. Therefore, the updated moving probability mechanism is given as follows

$$P_{ij}(t) = \frac{l_j(t) - l_i(t)}{\sum_{k \in N_t} l_k(t) - l_i(t)} \quad (8)$$

In Eq. (8),  $p_{ij}(t)$  denotes the probability with  $i$ -th glowworm relocates to glowworm  $j$  at  $t$  time. The upgraded glowworm location method can be represented as follows:

$$x_i(t+1) = x_i(t) + s \left( \frac{x_j(t) - x_i(t)}{\|x_j(t) - x_i(t)\|} \right) \quad (9)$$

Quantum computing was incorporated for improving the work process of the GSO system. Quantum computation is a computation method that uses suitable methods for a quantum theory such as estimation of quantum, along with state superposition. The core factor of quantum processing was qubit. The basic states  $|0\rangle$  and  $|1\rangle$  improve qubit which is demonstrated as linear integration of 2 primary states as given below,

$$|Q\rangle = \alpha|0\rangle + \beta|1\rangle \quad (10)$$

In Eq. (10),  $|\alpha|^2 + |\beta|^2 = 1$  where  $|\alpha|^2$  describes the observing state's possibility  $|0\rangle$ , and  $|\beta|^2$  denotes possibility of observing state  $|1\rangle$ . A quantum was deployed via  $n$  qubits. Lastly,  $n$ -qubits quantum can be represented as follows:

$$\Psi = \sum_{x=0}^{2^n-1} C_x |x\rangle, \quad \sum_{x=0}^{2^n-1} |C_x|^2 = 1 \quad (11)$$

By using the quantum gate, the qubit condition such as NOT, Hadamard, and rotation gates are modified. At first, the rotation gate can be represented as a mutation operator used to develop a quanta mechanism and better solution for identifying a globally optimum solution.

The rotation gate can be demonstrated in the following:

$$\begin{bmatrix} \alpha^d(t+1) \\ \beta^d(t+1) \end{bmatrix} = \begin{bmatrix} \cos(\Delta\theta^d) & -\sin(\Delta\theta^d) \\ \sin(\Delta\theta^d) & \cos(\Delta\theta^d) \end{bmatrix} \begin{bmatrix} \alpha^d(t) \\ \beta^d(t) \end{bmatrix} \text{ for } d = 1, 2, \dots, n \quad (12)$$

In Eq. (12),  $\Delta\theta^d = \Delta \times S(\alpha^d, \beta^d)$ ,  $\Delta\theta^d$  connotes the rotation angle of a qubit,  $\Delta$  and  $S(\alpha^d, \beta^d)$  indicates the magnitude and dimension of rotation subsequently.

The fitness choice is a critical feature of the QGSO model. The solution encoding is employed to evaluate the outcomes of the candidate goodness. At this moment, the accuracy value was the key factor implemented for planning a fitness function.

$$Fitness = \max(P) \quad (13)$$

$$P = \frac{TP}{TP + FP} \quad (14)$$

where,  $TP$  and  $FP$  implies the true and false positive values.

#### D. Image Classification

In the last phase, the QRNN method was employed for the accurate classifying of lung-associated diseases. All the layers of QRNN comprise two types of subcomponents, similar to pooling and convolution layers in CNN [20]. The convolution components such as the convolution layer in CNN enable fully parallel computation across both spatial dimensions and minibatch, in such cases sequence dimension. The pooling components such as the pooling layer in CNN, lack trainable parameter and enables fully parallel computation across feature dimensions and minibatch. Fig. 2 displays the construction of QRNN.

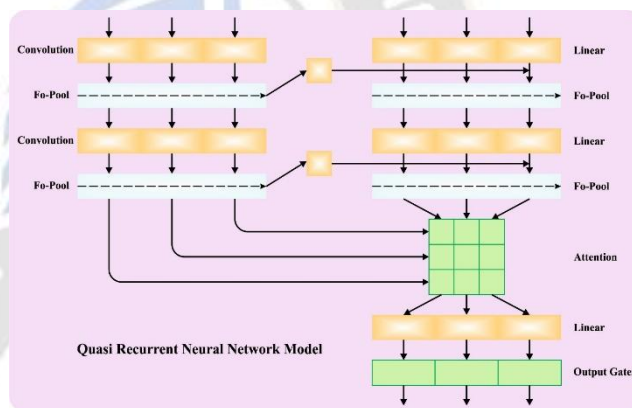


Figure 2. Structure of QRNN

Assume an input serial  $X \in \mathbb{R}^{T \times n}$  of  $T$   $n$ -dimensional vector  $x_1 \dots x_T$ , the convolution sub-components of QRNN perform convolution in the timestep dimension with a bank of  $m$  filters, generating a serial  $Z \in \mathbb{R}^{T \times m}$  of  $m$ -dimensional candidate vector  $z_t$ . Specifically, with filters of width  $k$ , every  $z_t$  relies on  $X_t - k + 1$  through  $x_t$ . Then, additional convolution is employed with a separate filter bank to accomplish a sequence of vectors for component-wise gates that are desired for the pooling function. If the pooling function needs an output gate  $O_t$  and forgets gate  $F_t$  at every timestep, the complete computation set in the complex element is given as follows:

$$\begin{aligned} Z &= \tanh(W_z * X) \\ F &= \sigma(W_f * X) \\ O &= \sigma(W_o * X) \end{aligned} \quad (15)$$

In Eq. (15),  $W_z$ ,  $W_f$ , and  $W_o$ , each in  $\mathbb{R}^{k \times n \times m}$ , denotes the convolution filter bank and  $*$  represents a mask convolution alongside the timestep dimension. It should be noted that if the filter width was 2, this equation is reduced to LSTM as

$$\begin{aligned} z_t &= \tanh(W_z^1 x_{t-1} + W_z^2 x_t) \\ f_t &= \sigma(W_f^1 x_{t-1} + W_f^2 x_t) \\ o_t &= \sigma(W_o^1 x_{t-1} + W_o^2 x_t) \end{aligned} \quad (16)$$

The appropriate function for the pooling sub-component is made from the component-wise gate of the conventional LSTM cells. Then, seek function controlled by the gate that could mix state across timestep where independently act on every state vector channel. The simple option, Balduzzi & Ghifary (2016) state “dynamic average pooling”, exploits only forget gate:

$$h_t = f_t \odot h_{t-1} + (1 - f_t) \odot z_t \quad (17)$$

In Eq. (17),  $\odot$  characterizes component-wise multiplication. Also, the function might include an output gate:

$$\begin{aligned} c_t &= f_t \odot c_{t-1} + (1 - f_t) \odot z_t \\ h_t &= o_t \odot c_t \end{aligned} \quad (18)$$

Or the recurrence relationship might embrace an independent forget and input gate:

$$\begin{aligned} c_t &= f_t \odot c_{t-1} + i_t \odot z_t \\ h_t &= o_t \odot c_t \end{aligned} \quad (19)$$

We initialize  $h$  or  $c$  to 0, We term 3 options  $f$ -pooling,  $f_o$ -pooling, and  $i$ fo-pooling correspondingly. Even though the recurrent part of this function should be successively computed for every timestep, their parallelism, and simplicity alongside feature dimension imply that, in real-time, estimating them over even longer sequences needs a limited number of computational time.

Thus, one QRNN layer implements an input-dependent pooling, then by the gated serial integration of the convolution feature. With CNNs, multiple QRNN layers must be stacked to generate a method with the capability for the approximation of complex functions.

#### IV. PERFORMANCE VALIDATION

The presented method is duplicated by implementing Python 3.6.5 tool on LAPTOP-EVV5KL7B, 8GB RAM, AMD Ryzen 5 3500U with Radeon Vega Mobile Gfx 2.10 GHz, 1TB HDD, and 250GB SSD. The set up of the parameter are represented in the following: rate of learning: 0.01, batch size: 5, dropout: 0.5, activation: ReLU, and epoch count: 50.

In this segment, the lung disease detection outputs of the QGSO-QRNN approach can be experimented on the radiography dataset [21] having 15153 sample values with three classes as illustrated in Table I. Fig. 3 demonstrates the instance imaging with their pre-processed versions.

Class	Number of Instances
COVID	3616
Normal	10192
Viral Pneumonia	1345
Total Number of Instances	15153

Fig. 4 represents the sample imaging. Fig. 4a shows the original CXR images and their respective masked regions are illustrated in Fig. 4b.

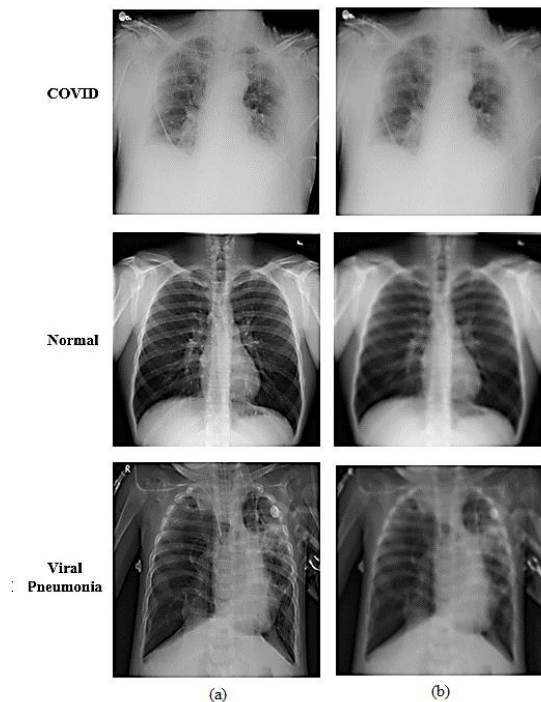


Figure 3. Sample images (a) Input, (b) Pre-processed

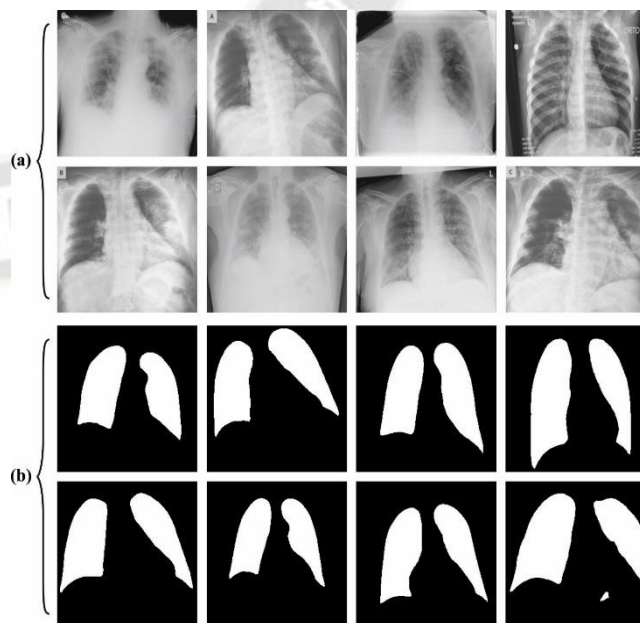


Figure 4. Sample images (a) Input (b) Masked

TABLE I. DATASET DETAILS

Fig. 5 shows the classifier outputs of the QGSO-QRNN model under the trial dataset. Fig. 5a portrays the confusion matrices rendered by the QGSO-QRNN model under 70% of TRS. The figure exhibited that the QGSO-QRNN approach has identified 2421 instances of COVID, 7060 instances under normal, and 833 instances under viral pneumonia. As well, Fig. 5b shows the confusion matrices offered by the QGSO-QRNN approach under 30% of TSS. The figure denoted that the QGSO-QRNN method has identified 1006 instances of COVID, 3020 instances under normal, and 382 instances under viral pneumonia. Similarly, Fig. 5c exhibits the PR investigation of the QGSO-QRNN approach. The figures reported that the QGSO-QRNN approach has obtained maximum PR achievement under the overall classes. Lastly, Fig. 5d shows the ROC investigation of the QGSO-QRNN technique. The figure depicted that the QGSO-QRNN method has advanced outputs with maximum values of ROC under discrete class labelling.

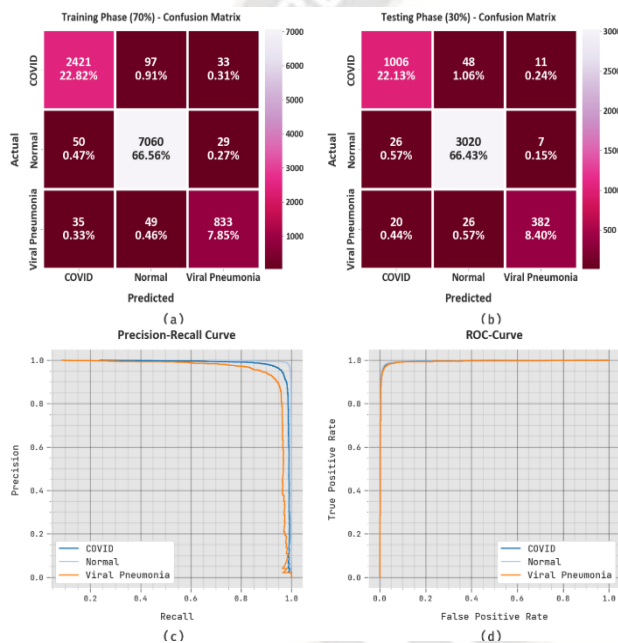


Figure 5. Classifiers of (a-b) 70:30 of TRS/TSS, (c-d) PR and ROC curve

Table II provides a short result analysis of the QGSO-QRNN method with 70:30 of TRS/TSS. The outputs indicate that the QGSO-QRNN method identifies lung diseases efficaciously. Fig. 6 portrays the overall lung disease detection results of the QGSO-QRNN technique on 70% of TRS. The outputs imply that the QGSO-QRNN technique attains improvised outputs under all classes. For example, in the COVID class, the QGSO-QRNN approach obtains an  $accu_y$  of 97.97%,  $prec_n$  of 96.61%,  $sens_y$  of 94.90%,  $spec_y$  of 98.94%,  $F_{score}$  of 95.75%, and MCC of 94.42%. Moreover, in the normal class, the QGSO-QRNN approach gains  $accu_y$  of 97.88%,  $prec_n$  of 97.97%,  $sens_y$  of 98.89%,  $spec_y$  of 95.79%,  $F_{score}$  of 98.43%, and MCC of 95.17%. Meanwhile, on the viral pneumonia class, the

QGSO-QRNN approach gains  $accu_y$  of 98.62%,  $prec_n$  of 93.07%,  $sens_y$  of 90.84%,  $spec_y$  of 99.36%,  $F_{score}$  of 91.94%, and MCC of 91.20%.

TABLE II. CLASSIFYING RESULT OF QGSO-QRNN ALGORITHM ON 70:30 OF TRS/TSS

Class	$Accu_y$	$Prec_n$	$Sens_y$	$Spec_y$	$F_{score}$	MCC
<b>Training Phase (70%)</b>						
COVID	97.97	96.61	94.90	98.94	95.75	94.42
Normal	97.88	97.97	98.89	95.79	98.43	95.17
Viral Pneumonia	98.62	93.07	90.84	99.36	91.94	91.20
<b>Average</b>	<b>98.16</b>	<b>95.88</b>	<b>94.88</b>	<b>98.03</b>	<b>95.37</b>	<b>93.60</b>
<b>Testing Phase (30%)</b>						
COVID	97.69	95.63	94.46	98.68	95.04	93.54
Normal	97.65	97.61	98.92	95.04	98.26	94.65
Viral Pneumonia	98.59	95.50	89.25	99.56	92.27	91.56
<b>Average</b>	<b>97.98</b>	<b>96.25</b>	<b>94.21</b>	<b>97.76</b>	<b>95.19</b>	<b>93.25</b>

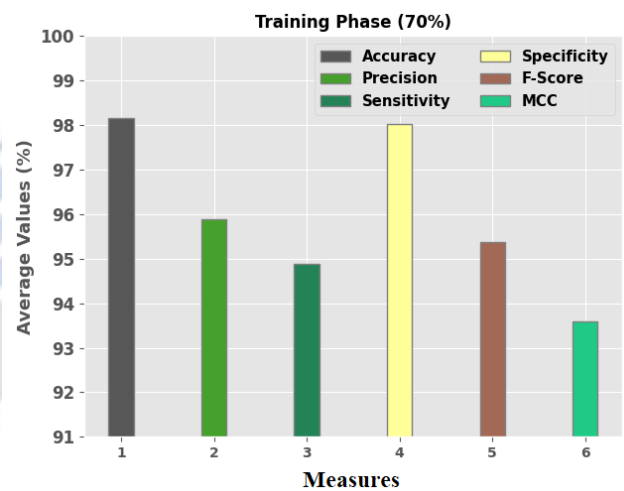


Figure 6. Performance analysis of QGSO-QRNN approach on 70% of TRS

Fig. 7 portrays the overall lung disease detection results of the QGSO-QRNN technique on 30% of TSS. The results imply that the QGSO-QRNN technique reaches improvised outputs under all classes. For instance, in the COVID class, the QGSO-QRNN approach gains  $accu_y$  of 97.69%,  $prec_n$  of 95.63%,  $sens_y$  of 94.46%,  $spec_y$  of 98.68%,  $F_{score}$  of 95.04%, and MCC of 93.54%. Also, in the normal class, the QGSO-QRNN approach gains  $accu_y$  of 97.65%,  $prec_n$  of 97.61%,  $sens_y$  of 98.92%,  $spec_y$  of 95.04%,  $F_{score}$  of 98.26%, and MCC of 94.65%. In the meantime, on viral pneumonia class, the QGSO-QRNN method obtains  $accu_y$  of 98.59%,  $prec_n$  of 95.50%,  $sens_y$  of 89.25%,  $spec_y$  of 99.56%,  $F_{score}$  of 92.27%, and MCC of 91.56%.

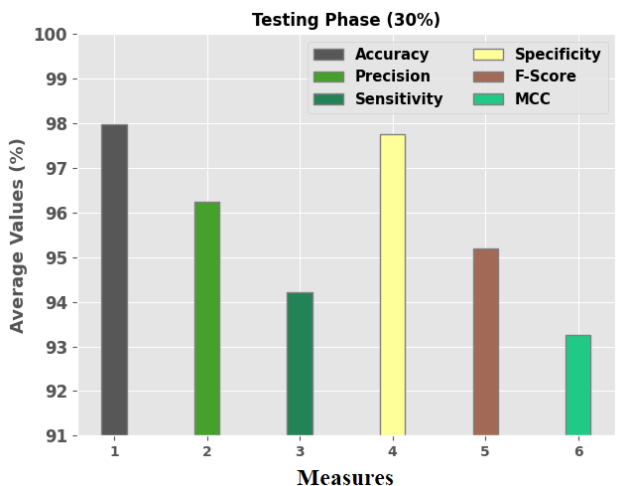


Figure 7. Performance evaluation of QGSO-QRNN model on 30% of TSS

The TACY value and VACY value of the QGSO-QRNN approach are experimented on lung ailment recognition achievement in Fig. 8. The figure outcomes that the QGSO-QRNN approach revealed augmented achievement with higher TACY and VACY values. Especially, the QGSO-QRNN approach has greater TACY outputs.

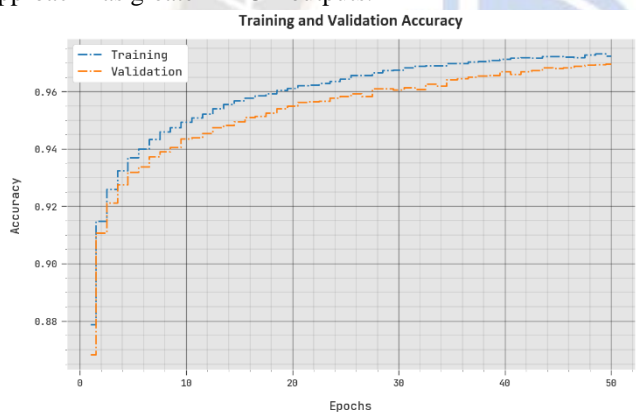


Figure 8. TACY and VACY output of QGSO-QRNN approach

The TLOS value and VLOS value of the QGSO-QRNN model are investigated on lung disease recognition achievement in Fig. 9. The figure revealed that the QGSO-QRNN approach has illustrated a better achievement with minimum TLOS and VLOS values. Visibly, the QGSO-QRNN approach has lessened VLOS results.

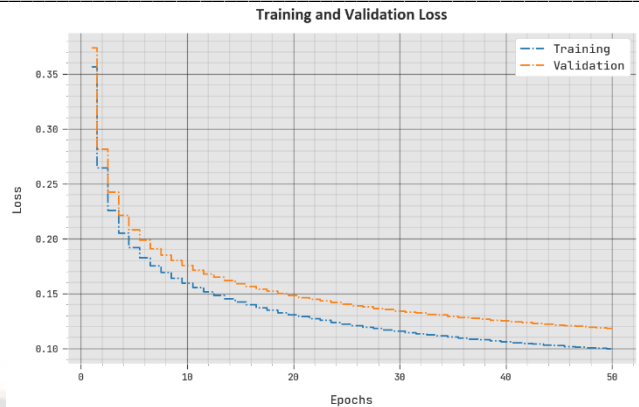


Figure 9. TLOS and VLOS output of QGSO-QRNN model

Table III exhibits an elaborated research of the QGSO-QRNN approach with present techniques [22].

TABLE III. RELATIVE OUTCOME OF QGSO-QRNN APPROACH WITH PRESENT SYSTEMS

Method	Accu <sub>y</sub>	Prec <sub>n</sub>	Sens <sub>y</sub>	Spec <sub>y</sub>	F <sub>Score</sub>
QGSO-QRNN	98.16	95.88	94.88	98.03	95.37
Non-optimization	90.22	82.10	93.89	89.68	87.71
Genetic Algorithm	94.89	91.31	92.80	92.43	95.09
Pattern search	94.82	87.43	94.02	93.62	93.51
Simulated Annealing	95.24	94.76	94.11	92.62	92.62
PSO Algorithm	95.16	89.76	92.70	95.22	93.13
WO Algorithm	96.43	94.19	93.35	93.98	94.95
OptCoNet	97.30	95.14	94.20	97.43	94.74

Fig. 10 demonstrates a comparative  $accu_y$  examination of the QGSO-QRNN technique with existing models. Based on  $accu_y$ , the experimental values represent that the QGSO-QRNN technique attains an improved  $accu_y$  of 98.16% while the NO, GA, PS, SA, PSO, WO, and OptCoNet techniques accomplish reduced  $accu_y$  of 90.22%, 94.89%, 94.82%, 95.24%, 95.16%, 96.43%, and 97.30% subsequently.

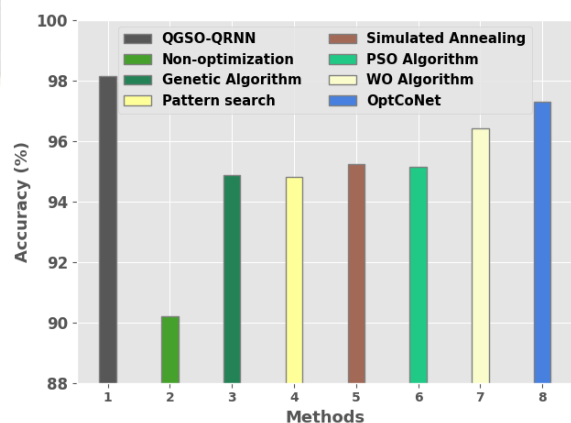


Figure 10. Accu<sub>y</sub> outcome of QGSO-QRNN approach with existing systems

Fig. 11 shows a comparative  $prec_n$  and  $F_{score}$  examination of the QGSO-QRNN technique with existing methods. Based on  $prec_n$ , the experimental values indicate that the QGSO-QRNN technique reaches an improved  $prec_n$  of 95.88% while the NO, GA, PS, SA, PSO, WO, and OptCoNet techniques accomplish reduced  $prec_n$  of 82.10%, 91.31%, 87.43%, 94.76%, 89.76%, 94.19%, and 95.14% correspondingly. Eventually, based on  $F_{score}$ , the experimental values indicate that the QGSO-QRNN technique reaches an improved  $F_{score}$  of 95.37% while the NO, GA, PS, SA, PSO, WO, and OptCoNet methods accomplish a reduced  $F_{score}$  of 87.71%, 95.09%, 93.51%, 92.62%, 93.13%, 94.95%, and 94.74% correspondingly.

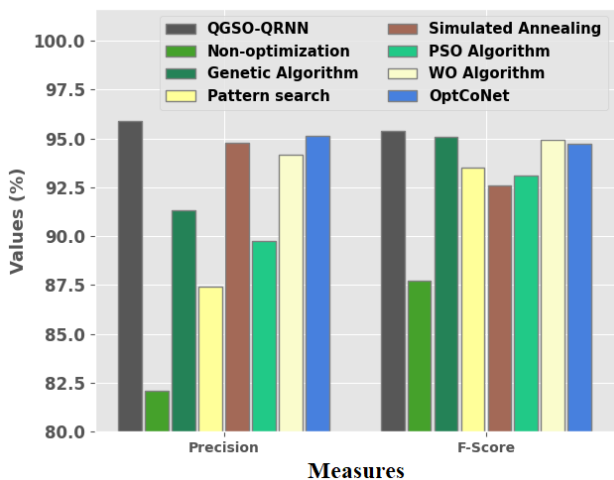


Figure 11.  $prec_n$  and  $F_{score}$  outcome of QGSO-QRNN approach with existing systems

Fig. 12 exhibits a relative  $sens_y$  and  $spec_y$  examination of the QGSO-QRNN technique with existing methods. Based on  $sens_y$ , the experimental values specify that the technique reaches an improved  $sens_y$  of 94.88% while the NO, GA, PS, SA, PSO, WO, and OptCoNet methods accomplish reduced  $sens_y$  of 93.89%, 92.80%, 94.02%, 94.11%, 92.70%, 93.35%, and 94.20% correspondingly. Eventually, based on  $spec_y$ , the experimental values indicate that the QGSO-QRNN method reaches an improved  $spec_y$  of 98.03% while the NO, GA, PS, SA, PSO, WO, and OptCoNet method reduced  $spec_y$  of 89.68%, 92.43%, 93.62%, 92.62%, 95.22%, 93.98%, and 97.43% correspondingly.

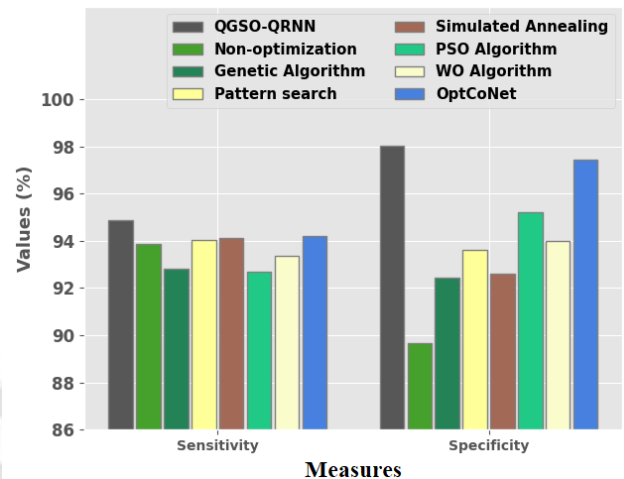


Figure 12.  $sens_y$  and  $spec_y$  outcome of QGSO-QRNN approach with existing systems

Table IV and Fig. 13 illustrate the comparative QGSO-QRNN model with other existing approaches by means of CT. The outputs represent that the QGSO-QRNN model accomplishes effective performance with a minimum CT value of 8.06s. On the other hand, the NO, GA, PS, SA, PSO, WO, and OptCoNet methods accomplish increased CT of 11.05s, 10.45s, 10.01s, 13.10s, 11.43s, 12.03s, and 14.05s respectively.

TABLE IV. RELATIVE CT OF QGSO-QRNN MODEL WITH PRESENT SYSTEMS

Methods	Computational Time (Sec)
QGSO-QRNN	08.06
Non-optimization	11.05
Genetic Algorithm	10.45
Pattern search	10.01
Simulated Annealing	13.10
PSO Algorithm	11.43
WO Algorithm	12.03
OptCoNet	14.05

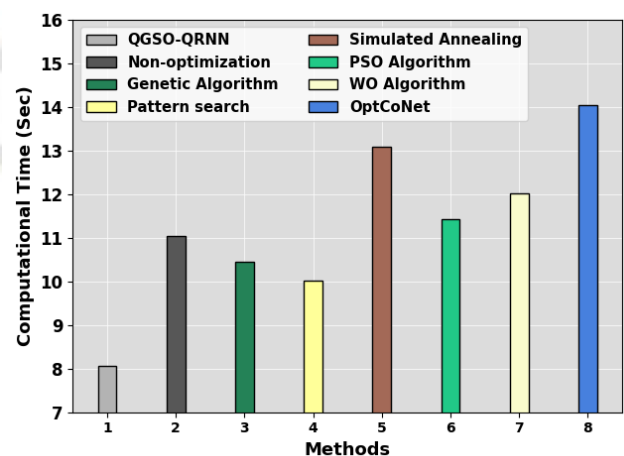


Figure 13. CT comparison of QGSO-QRNN approach with existing systems

These outputs demonstrated the improved achievement of the QGSO-QRNN model over other current approaches.

## V. CONCLUSION

In this research, we have developed a new QGSO-QRNN model for identifying and classifying lung diseases on the CXR images. The presented QGSO-QRNN model primarily pre-processed the input imaging through the GF method. Moreover, the Faster SqueezeNet method is used for effectually generating the feature vector. Finally, the QRNN method can be employed to accurately identify lung diseases and the QGSO technique was used as a hyperparameter optimizer. The experimental validation of the QGSO-QRNN technique can be investigated by employing benchmark medical datasets and the outcomes display the promising performance of the QGSO-QRNN methodology over other existing techniques in terms of diverse measures. In the coming days, advanced DL classification approaches can enhance the performance of the QGSO-QRNN methodology.

## REFERENCES

- [1] Soni, M., Gomathi, S., Kumar, P., Churi, P.P., Mohammed, M.A. and Salman, A.O., 2022. Hybridizing convolutional neural network for classification of lung diseases. *International Journal of Swarm Intelligence Research (IJSIR)*, 13(2), pp.1-15.
- [2] Soffer, S., Morgenthau, A.S., Shimon, O., Barash, Y., Konen, E., Glicksberg, B.S. and Klang, E., 2022. Artificial intelligence for interstitial lung disease analysis on chest computed tomography: a systematic review. *Academic Radiology*, 29, pp.S226-S235.
- [3] Ravi, V., Narasimhan, H., Chakraborty, C. and Pham, T.D., 2022. Deep learning-based meta-classifier approach for COVID-19 classification using CT scan and chest X-ray images. *Multimedia systems*, 28(4), pp.1401-1415.
- [4] Hussein, F., Mughaid, A., AlZu'bi, S., El-Salhi, S.M., Abuhajja, B., Abualigah, L. and Gandomi, A.H., 2022. Hybrid CLAHE-CNN Deep Neural Networks for Classifying Lung Diseases from X-ray Acquisitions. *Electronics*, 11(19), p.3075.
- [5] Bortoluzzi, E.M., Schmidt, P.H., Brown, R.E., Jensen, M., Mancke, M.R., Larson, R.L., Lancaster, P.A. and White, B.J., 2023. Image Classification and Automated Machine Learning to Classify Lung Pathologies in Deceased Feedlot Cattle. *Veterinary Sciences*, 10(2), p.113.
- [6] Kasinathan, G. and Jayakumar, S., 2022. Cloud-based lung tumour detection and stage classification using deep learning techniques. *BioMed Research International*, 2022.
- [7] Aggarwal, P., Mishra, N.K., Fatimah, B., Singh, P., Gupta, A. and Joshi, S.D., 2022. COVID-19 image classification using deep learning: Advances, challenges, and opportunities. *Computers in Biology and Medicine*, p.105350.
- [8] Sun, J., Liao, X., Yan, Y., Zhang, X., Sun, J., Tan, W., Liu, B., Wu, J., Guo, Q., Gao, S. and Li, Z., 2022. Detection and staging of chronic obstructive pulmonary disease using a computed tomography-based weakly supervised deep learning approach. *European Radiology*, 32(8), pp.5319-5329.
- [9] Petmezas, G., Cheimariotis, G.A., Stefanopoulos, L., Rocha, B., Paiva, R.P., Katsaggelos, A.K. and Maglaveras, N., 2022. Automated lung sound classification using a hybrid CNN-LSTM network and focal loss function. *Sensors*, 22(3), p.1232.
- [10] Shamrat, F.J.M., Azam, S., Karim, A., Islam, R., Tasnim, Z., Ghosh, P. and De Boer, F., 2022. LungNet22: A Fine-Tuned Model for Multiclass Classification and Prediction of Lung Disease Using X-ray Images. *Journal of Personalized Medicine*, 12(5), p.680.
- [11] Indumathi, V. and Siva, R., 2023. An efficient lung disease classification from X-ray images using hybrid Mask-RCNN and BiDLSTM. *Biomedical Signal Processing and Control*, 81, p.104340.
- [12] Kim, S., Rim, B., Choi, S., Lee, A., Min, S. and Hong, M., 2022. Deep learning in multi-class lung diseases' classification on chest X-ray images. *Diagnostics*, 12(4), p.915.
- [13] Ravi, V., Acharya, V. and Alazab, M., 2022. A multichannel EfficientNet deep learning-based stacking ensemble approach for lung disease detection using chest X-ray images. *Cluster Computing*, pp.1-23.
- [14] Kabiraj, A., Meena, T., Reddy, P.B. and Roy, S., 2022, December. Detection and Classification of Lung Disease Using Deep Learning Architecture from X-ray Images. In *Advances in Visual Computing: 17th International Symposium, ISVC 2022, San Diego, CA, USA, October 3–5, 2022, Proceedings, Part I* (pp. 444-455). Cham: Springer International Publishing.
- [15] Alshmrani, G.M.M., Ni, Q., Jiang, R., Pervaiz, H. and Elshennawy, N.M., 2023. A deep learning architecture for multi-class lung disease classification using chest X-ray (CXR) images. *Alexandria Engineering Journal*, 64, pp.923-935.
- [16] Wang, B. and Zhang, W., 2022. MARnet: Multi-scale adaptive residual neural network for chest X-ray images recognition of lung diseases. *Math. Biosci. Eng.*, 19(1), pp.331-350.
- [17] Bharati, S., Khan, T.Z., Podder, P. and Hung, N.Q., 2021. A comparative analysis of image denoising problem: noise models, denoising filters and applications. In *Cognitive Internet of Medical Things for Smart Healthcare* (pp. 49-66). Springer, Cham.
- [18] Xu, Y., Yang, G., Luo, J. and He, J., 2020. n Electronic component recognition algorithm based on deep learning with a faster SqueezeNet. *Mathematical Problems in Engineering*, 2020, pp.1-11.
- [19] Sampathkumar, A., Mulerikkal, J. and Sivaram, M., 2020. Glowworm swarm optimization for effectual load balancing and routing strategies in wireless sensor networks. *Wireless Networks*, 26, pp.4227-4238.
- [20] Bradbury, J., Merity, S., Xiong, C. and Socher, R., 2016. Quasi-recurrent neural networks. *arXiv preprint arXiv:1611.01576*.

- [21] <https://www.kaggle.com/datasets/tawsifurrahman/covid19-radiography-database/code>
- [22] Goel, T., Murugan, R., Mirjalili, S. and Chakrabarty, D.K., 2021. OptCoNet: an optimized convolutional neural network for an automatic diagnosis of COVID-19. *Applied Intelligence*, 51, pp.1351-1366

